Applied Catalysis B: Environmental 284 (2021) 119743

Contents lists available at ScienceDirect

Applied Catalysis B: Environmental

journal homepage: www.elsevier.com/locate/apcatb

Real time imaging of photocatalytic active site formation during H_2 evolution by in-situ TEM

Shuohan Yu [a], Youhong Jiang [b], Yue Sun [b], Fei Gao [a,*], Weixin Zou [a], Honggang Liao [b,*], Lin Dong [a,*]

[a] Jiangsu Key Laboratory of Vehicle Emissions Control, School of the Environment, Center of Modern Analysis, Key Laboratory of Mesoscopic Chemistry of MOE, School of Chemistry and Chemical Engineering, Nanjing University, Nanjing 210093, PR China
[b] College of Chemistry and Chemical Engineering, Xiamen University, Xiamen 361005, PR China

ARTICLE INFO

Keywords:
In situ TEM
Heterogeneous catalysts
Active sites
Catalytic mechanism
Photocatalysis

ABSTRACT

The understanding of reaction mechanism is the theoretical premise for all the industrial improvement of catalysts. However, off-line characterization may mislead the study of catalytic mechanism if the catalyst itself is unstable during reaction. In this work, in-situ transmission electron microscopy (TEM) was emploied to investigate the photocatalysis process of H_2 evolution on Cu_2O. Real time imaging identified the self-reduction of Cu_2O to nano-Cu on particle surface and its catalytic activity was come from the self reduced nano-Cu. Further quantification results indicated that the degree of Cu_2O self-reduction was highly matched with the Cu_2O catalytic activity. The in-situ TEM here for the first time confirmed the in-situ formation of active site under reaction condition, these finding may beneficial for future catalyst design.

1. Introduction

Understanding how nanomaterials catalyse chemical reactions is important for the development of efficient catalytic materials for a wide range of energy and environmental technologies [1–7]. These nano-sized materials generally expose different surface sites with distinct reactivity for the turnover of reactants. The identification and characterization of the surface active sites or the site-specific reactivity is therefore attracting extensive attention in recent years [8–12]. However, nano-sized catalysts often respond dynamically to the reaction environment or stimuli, because changes in the reaction environment affect the free energy of the exposed surfaces site. The surface structure, composition and reactivity are therefore related to the reaction conditions, thus, the identification of active sites and their properties in-situ during catalysis is extremely important. Although many in-situ and operando techniques are available, [13–17] it remains a challenge to obtain structure and composition of the active site of nanomaterials under real reaction environment and stimuli at atomic-scale.

Heterogeneous catalysts are widely used in fields of energy, environment, and chemical industry [1, 2, 4–7]. The study of active sites is one of the key points of relative researches [1,4,9,11]. Based on a precise molecular understanding of the active sites, improving the selectivity and activity of these complex catalyst systems can be undertaken through the powerful structure–reactivity approach [18–21]. However, recent studies have shown that many catalysts are unstable during working. For instance, Ostwald ripening of Pt on carbon and the migration of soluble platinum species cause the platinum area loss of the Pt/C electrocatalysts in proton exchange membrane fuel cells.[22] Hydrogen and water lead to Pt agglomeration and redispersion in Pt/Al_2O_3 catalyst. [23] In the photocatalytic reaction of some semiconductor catalysts, such as ZnO, $BiVO_4$, et al., [24–27] oxygen defects occur on the surface of the catalysts, which leads to the corrosion of the catalysts. In these changes of catalysts, the active sites correspondingly varied in migration, agglomeration and reconstruction, which brought obstacles to the characterization of the active sites.

Recently, the development of a liquid cell TEM enables the direct observation of nanoscale chemical reactions and the physical changes in a solution. With the aid of liquid cell chips, Zheng's group [28,29] has realized in-situ TEM observation of colloid nanoparticles formation in solution. Liquid cell technology can avoid the influence of TEM vacuum system by sealing the atmosphere or liquid inside the chip. Hence it is feasible to simulate such a liquid/gas reaction inside TEM. However, the difficulty of the introduction of light source into the small space in liquid cell between the TEM pole pieces make photo induced in-situ TEM

* Corresponding author.
E-mail addresses: gaofei@nju.edu.cn (F. Gao), hgliao@xmu.edu.cn (H. Liao), donglin@nju.edu.cn (L. Dong).

https://doi.org/10.1016/j.apcatb.2020.119743
Received 18 September 2020; Received in revised form 2 November 2020; Accepted 6 November 2020
Available online 24 November 2020

studies hardly be reported until very recently. In order to conquer this problem, Yin and co-workers [30] employed the electron beam mimic a "light" source to initiate the water splitting on TiO_2 nano-rods. However, electron beams are not completely equivalent to natural light. In Sui's report, [31] light was introduce by the modify TEM and a regular liquid TEM holder was employed to investigate the photocatalytic water splitting on TiO_2, but the modification of TEM is very expensive and complicated.

In this work, for the first time, we achieved the direct TEM observation of photocatalytic reaction on instable Cu_2O catalyst through a homemade in-situ TEM holder and liquid cell. Cu_2O catalyst in-situ structure change during light induced hydrogen production was captured. It was proved that surface layer of Cu_2O cube was self-reduced to nano-Cu. Further quantitative analysis indicates that the degree of Cu_2O self-reduction was highly matched with the photocatalytic hydrogen production rate. In this work, the role in-situ formation of active site on nanocatalyst during the photocatalytic hydrogen production was first identified and investigated by in-situ TEM, which brings a new method for further understanding catalysis mechanism of catalyst.

2. Experimental details

2.1. Preparation of Cu_2O nanoparticles

Cu_2O nanoparticles with uniform size were prepared by seed method [32]. Typically (Figure S1), aqueous solution was prepared containing copper sulfate (1.0×10^{-3} M) and sodium dodecyl sulfate (SDS, 3.3×10^{-2} M). Transfer 10 mL mixed solution into 50 mL centrifuge tube and mark as A. Three parts of 9 mL mixed solution were transferred into another three 50 mL centrifugal tubes, marked as B, C and D. Add 250 u L sodium ascorbate solution (SA, 0.2 M) to A and rotate for 5 s. Then add 500 u L NaOH water solution (1 M) and shake for another 5 s. The solution quickly turns yellow. Immediately transfer 1 mL solution from A to B as seed and rotate for 10 s. Repeat the previous operation of A, add 250 μL sodium ascorbate aqueous solution (0.2 M), shake for 5 s, then add 500 μL NaOH aqueous solution (1 M), shake for 5 s. Immediately transfer 1 mL of further growing seed solution from B to C, and rotate for 10 s. The same process was repeated for the preparation of C and D. After the completion of all operations, aging 2 h. The yellow precipitate in D was separated by centrifugation and washed with ethanol and deionized water for 3 times respectively. Finally, the solid product was dispersed in 10 mL of deionized water, and was signed as dispersion D. For XRD analysis, dispersion D was centrifuged and the yellow precipitate dried at 60 °C in vacuum overnight.

2.2. Characterizations

The X-ray diffraction (XRD) patterns of the catalysts were checked using an XRD-6000 X-ray diffractometer (Shimadzu).

The electron paramagnetic resonance (EPR) signal was examined at 77 K on EPR JES FA200 (JEOL) spectrometer.

Atomic absorption spectroscopy (AAS, analytik jena novAA350/ZEEnit650p) was employed to measure the concentration of Cu, Ag ions in catalyst digestion solution.

Off-line and in-situ transmission electron microscopy (TEM) experiments were carried out on a JEM-2100 instrument operated at 200 kV. HAADF-STEM images were obtained on a Talos F200 s instrument under STEM mode at 200 kV. The introduction of liquid in TEM system was realized by a liquid cell chip, and light was introduced by a modified TEM holder with an optical fiber through it. A high-power Xenon light source (Ocean Optics, HPX-2000) was employed as an external light source, and was connected to TEM holder through a SMA905 optical fiber patch cord. The light intensity at viewing window of liquid cell was about 120 mW/cm^2. It should be noted that in order to minimize the effect of electron beam and avoid reduction by it, we only turn the beam on 0.1 s during image acquisition, and the electron beam remained blanked within four hours of illumination. The amount of electron beam irradiation was 3 e/Å^2/s in in-situ TEM experiments. Extra experimental details for in-situ TEM, qualitative and quantitative analysis of Cu_2O self-reduction (Scheme S1) were showed in supporting information.

2.3. Photocatalytic H_2 generation test

The photocatalytic hydrogen evolution reactions were carried out in a top-irradiation type vessel linked to a gasclosed glass system (Ceaulight CEL-SPH2N-D, Ceaulight, Beijing, China) under an irradiation of the 300 W Xe lamp with the 420 nm cut-off filter. Dispersion D (10 mL), H_2O (80 mL), and ethanol (10 mL) were mixed in a quartz reactor. N_2 bubbling for 1 h, followed by vacuuming to maintain anaerobic conditions in the system. The temperature of the solution was kept around 6 °C. The amount of generated hydrogen was automatically collected and determined by using an online gas chromatograph equipped with a thermal conductive detector. Argon was used as the carrier gas for gas chromatography. The mass of Cu_2O was 0.5 mg (supplementary information, measurement of mass of Cu_2O in dispersion D).

2.4. Computational method

The density functional theory (DFT) calculations were carried out by the Vienna Ab-initio Simulation Package [33,34] (VASP), taking advantage of the Projected Augmented Wave [35] (PAW) method. The Perdew-Burke-Ernzerhof (RPBE) functional was used to describe the exchange and correlation effects [36]. For all the geometry optimizations, the cutoff energy was set to be 500 eV. The Monkhorst-Pack grids [37] were set to be $9 \times 9 \times 9$ and $4 \times 4 \times 1$ for performing the calculations of bulk and surface Cu_2O, respectively. A 20 Å vacuum thickness was added in the z-direction of the simulation box, preventing the interactions between the adjacent slabs.

3. Result and discussions

3.1. Structure of fresh Cu_2O

Cu_2O is a p-type semiconductor with high carrier mobility, which has satisfactory H_2 generation activity. [38] Cu element in Cu_2O has +1 valence, thus the catalyst has two possible transformation paths in the photocatalytic H_2 generation process: self-oxidation or self-reduction. Kakuta et al. [39] believed that Cu_2O was easily oxidized to CuO under light conditions, which led to catalyst inactivation. Toe et al. [40] systematically studied the effects of photogenic electrons and holes on the stability of Cu_2O in photocatalytic H_2 generation process and obtained similar conclusions. In contrast, some researchers believed that Cu_2O was reduced to Cu by accumulating photogenic electrons under light illumination. [41,42] Formation of Cu was considered to be unfavorable to the photocatalytic hydrogen generation reaction on Cu_2O catalyst. [38,41] It seems that whether self-reduction or self-oxidation occurs, it is not conducive to the hydrogen production reaction on the Cu_2O catalyst. However, in Zhen's work, [43] Cu as a co-catalyst was added to Cu_2O catalyst, and the catalytic activity of catalysts increased significantly. Cu was believed to improve the photoelectron transfer efficiency in the catalyst, thus promoting the catalyst activity. Similar phenomena has also been reported by Lou. [44] They believed the localized surface plasmon resonance effect of nano-copper contributed to the photocatalytic H_2 production reaction on Cu_2O catalyst. So far, it is still controversial whether self-reduction or self-oxidation of Cu_2O is dominant, and whether change of Cu_2O is beneficial or harmful to the photocatalytic hydrogen production.

According to literatures, [45] the charge separation efficiency on various exposed facets of Cu_2O is different, which leads to the anisotropic catalytic activity of Cu_2O. Therefore, to study the photocatalytic hydrogen production process on Cu_2O, we need to prepare Cu_2O nanoparticles with uniform and controllable structure to avoid

introducing too many variables. In this work, Cu_2O nanoparticles with uniform size were prepared by crystal seed method. [32] As shown in Fig. 1a-b, the X-ray diffraction (XRD) and selected area electron diffraction (SAED) patterns showed that the prepared sample had a single Cu_2O phase without other impurities. TEM images (Fig. 1c) confirmed that the morphology of Cu_2O samples was nanocube with side length of 140 nm. In the locally magnified TEM image (Fig. 1d), it was observed that the crystal lattice stripes parallel and perpendicular to the eight exposed surfaces of the Cu_2O cube were all 0.214 nm, belonging to the Cu_2O {200} facets. Therefore, it was determined that the 6 exposed surfaces of the Cu_2O cubes were all Cu_2O {100} facets. The Cu_2O edge section had an angle of 45° with the exposed Cu_2O {100} crystal planes, which indicated that 12 edges of Cu_2O cubes exposed Cu_2O {110} facets. According to the results of scanning electron microscopy (SEM, Fig. 1e), in addition to the exposed {100} and {110} facets, there was the third kind of exposed facets on the eight vertexes of the Cu_2O cubes. Since Cu_2O belonged to the cubic syngony, and the Cu_2O particles in the SEM and TEM images were uniform cubes, thus the vertex of Cu_2O was exposed {111} facet. Based on the analysis above, pure Cu_2O particles have been successfully synthesized, of which the morphologies are uniform cubes with side length of 140 nm, and exposed {100}, {110} and {111} facets (Fig. 1f).

3.2. Self-oxidation or self-reduction

Since the size of Cu_2O cubes are about 140 nm, the size of Cu or CuO generated owing to the possible self-reduction or self-oxidation during photocatalytic H_2 production will be smaller. Such a small Cu can be easily oxidized to CuO in air. Therefore, predictably, the off-line experiment exposed in air will seriously interfere with the understanding of the structural changes of Cu_2O in photocatalytic H_2 generation process. In order to avoid the interference of air, in-situ TEM analysis was employed. In-situ TEM instrument contains liquid cell chips and a modified TEM holder (Fig. 2). Light is introduced into the in-situ TEM system by modifying the TEM holder with an optical fiber through it (Fig. 2a-c). One end of the optical fiber is processed into a concave mirror, which focuses the light to the viewing window of the liquid cell chip. The liquid cell (Fig. 2d-e) is composed of top and bottom chip, between which a cavity with thickness of 200 nm is sealed to place the TEM sample. The small window in the center of the chip is a TEM viewing window (10 μm × 100 μm), through which the electron beam can image the sample. The viewing window is sealed by silicon nitride film about 10 nm thick. In this work, simulated reaction solution containing cuprous oxide (H_2O:EtOH = 9:1) was injected into liquid cell chip by capillary tube and sealed (supplementary information, in-situ TEM section).

As showed in Fig. 3a, Cu_2O cubes were separated in the liquid cell. The SAED result (Fig. 3d) showed that the fresh Cu_2O sample was a single crystal phase of Cu_2O. The liquid cell with reaction solution sealed in it was then illuminated for 4 h. Due to the reducibility of the electron beam, the electron beam was blanked during illumination to avoid the influence of the electron beam on Cu_2O except imaging. Within 4 h of illumination, the morphologies of Cu_2O cubes were basically unchanged (Fig. 3a-c, g, h). However, diffraction spots of metal Cu gradually

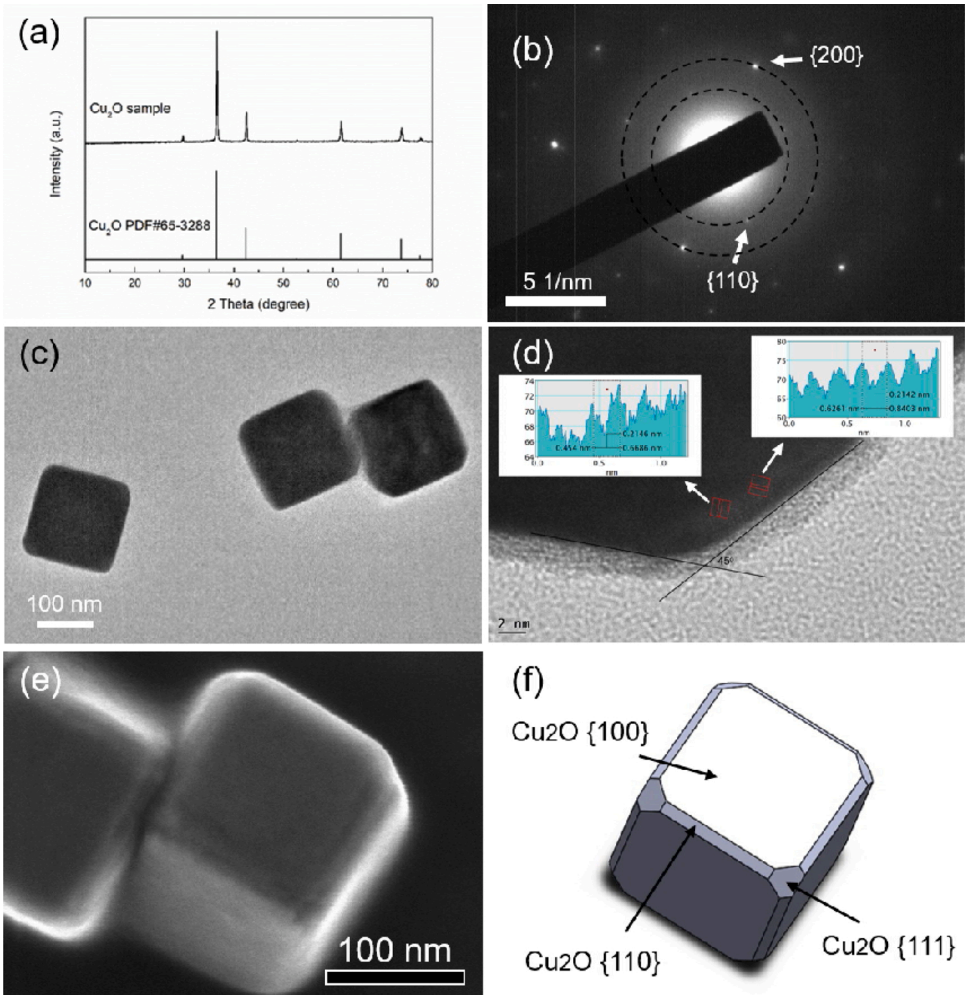

Fig. 1. (a) XRD pattern, (b) SEAD pattern, (c, d) TEM images, (e) SEM image, and (f) schematic diagram of Cu_2O cubes.

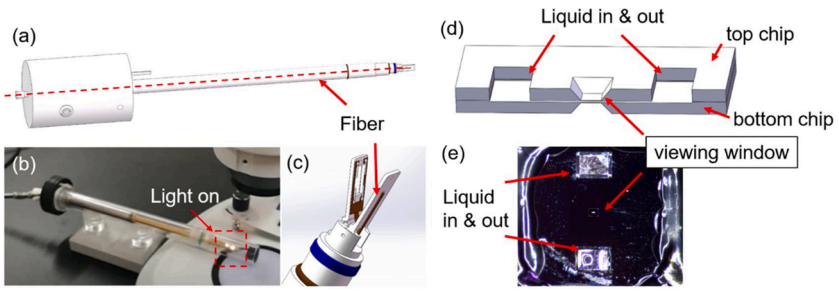

Fig. 2. Modified TEM holder with an optical fiber through it: (a, c) schematic diagrams, (b) real photo, and liquid cell chip: (d) schematic diagram, (e) real photo.

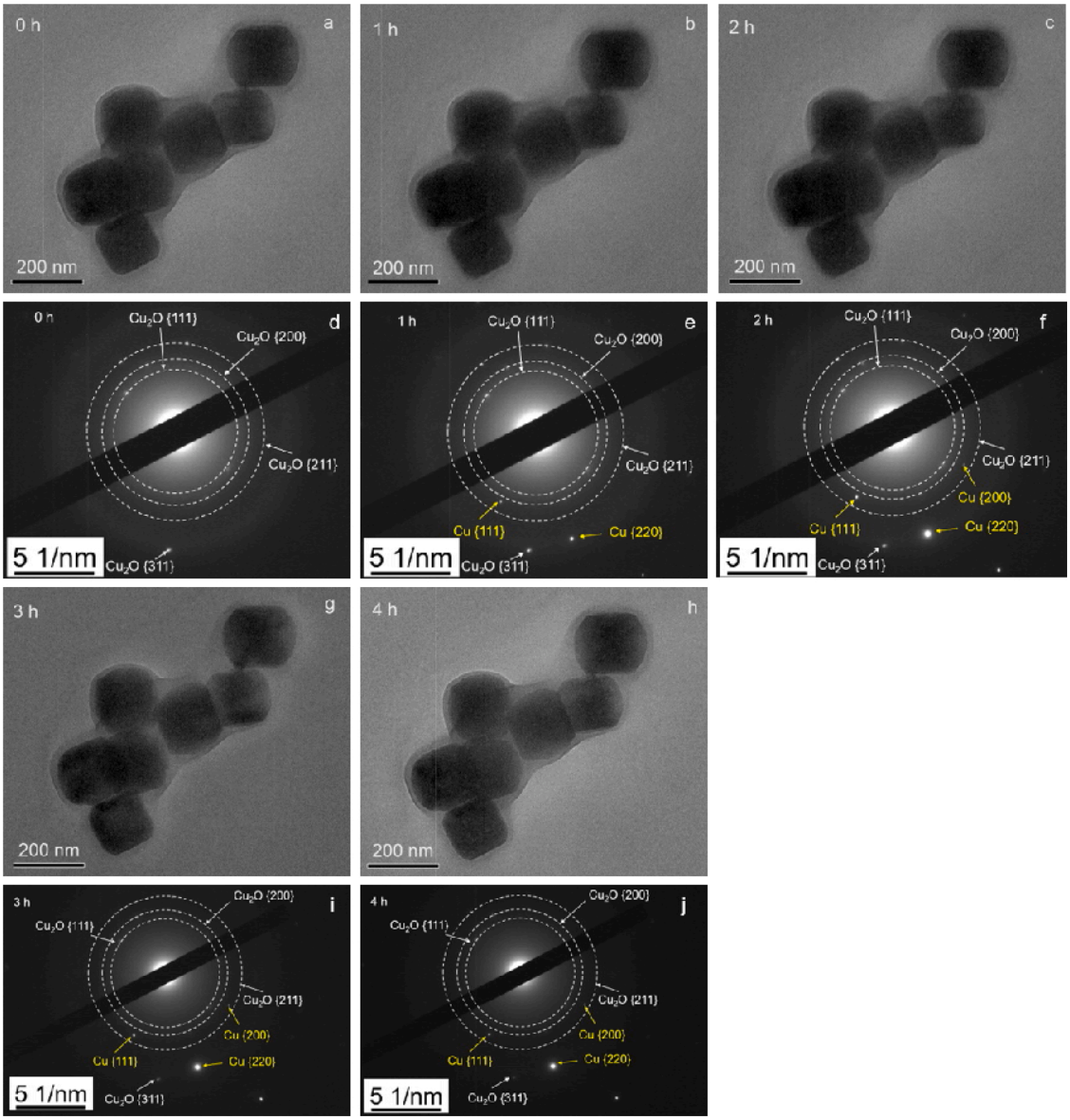

Fig. 3. In-situ TEM observation of Cu_2O in photocatalytic H_2 evolution process: (a, b, c, g, h) TEM images and (d, e, f, i, j) SAED patterns. (The stimulated reaction solution was a mixture of dispersion D sample and ethanol, where the ratio of ethanol to water by volume is 1:9. The light intensity at viewing window of liquid cell was about 120 mW/cm^2. In order to avoid electron beam effect, beam was only turned on 0.1 s when acquiring images.).

appeared in the SAED patterns with the duration of illumination (Fig. 3b-f, i, j), which directly proved that Cu_2O reduced to Cu.

In the presence of aqueous solution, Cu_2O is sensitive to electron irradiation dose. Therefore, in order to further observe the change of Cu_2O self-reduction with different light shining time, we emptied the liquid in the liquid cell at certain time, and HRTEM characterization was performed on the local structure of Cu_2O after light. As shown in Fig. 4, the morphologies of Cu_2O cubes hardly changed within 1 h of illumination. When the light lasted for 2 h, the surface of Cu_2O gradually became rough, and Cu particles first appeared in the corner (Fig. 4b).

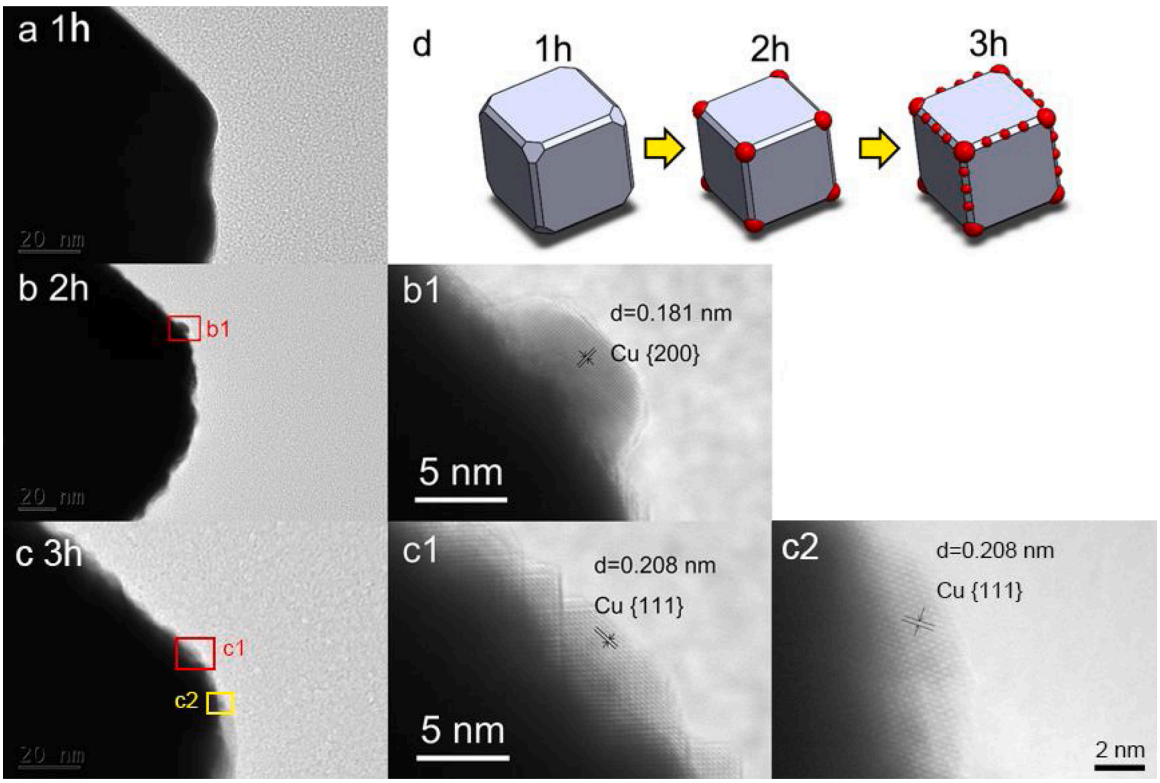

Fig. 4. HRTEM images of Cu_2O samples with different irradiated time: (a) 1 h, (b) 2 h, (c) 3 h, and schematic diagrams of (d) Cu_2O structure change under irradiation.

When the illumination continued for 3 h, Cu on Cu_2O surface spread from the corner to the edge of Cu_2O cubes (Fig. 4c).

In order to further verify the generation of Cu, we exposed the Cu_2O with reaction solution to light for 4 h under the protection of inert atmosphere, then injected $AgNO_3$ solution into the system after turning off the light (supplementary information, qualitative and quantitative analysis of Cu_2O self-reduction). The color of the simulated reaction solution after illumination changed from yellow to black rapidly, when $AgNO_3$ solution was injected (Figure S2a-b). Both CuO and Cu_2O are inert to $AgNO_3$, whereas Cu can reduce Ag^+ to Ag, of which the nanoparticles are black. The change of reaction solution color indicates that Cu_2O self-reduced to Cu in the process of photocatalytic hydrogen production. Owing to the limited observation area of TEM, the possibility of Cu_2O self-oxidation could not be completely excluded according to above results. Electron paramagnetic resonance (EPR) test was conducted to explore whether self-oxidation occurred. As showed in Figure S2c, both the fresh Cu_2O sample and the metal Cu have no EPR signal. For the CuO sample, EPR signal of Cu^{2+} was detected ($g_{\perp} = 2.07$), [46] as the Cu^{2+} electron structure is $[Ar]3d^9$ with a single electron. After the light was turned on, we sampled the simulated reaction solution every 1 h. There was no EPR signal of Cu^{2+} in the simulated reaction solution during the 4 h illumination, which indicated that the self-oxidation of Cu_2O did not occur in the process of photocatalytic hydrogen production. Interestingly, the EPR signal of Cu^{2+} appeared when air was pumped into the reaction solution after illumination, which indicated that the Cu self-reduced by Cu_2O in photocatalytic hydrogen production could be oxidized by air, which proving that the in-situ observation of the dynamic change of the catalyst is necessary.

3.3. How did self-reduction happen

In order to understand the process of Cu_2O self-reduction, the illuminated Cu_2O samples were treated by $AgNO_3$ to avoid the oxidation of nano-copper in air. By measuring the ratio of Ag and Cu through atomic absorption spectroscopy (AAS) analysis (supplementary information, structural and quantitative analysis of Cu_2O self-reduction), the self-reduction degree of Cu_2O can be quantified. It was found that Cu_2O quickly reduced under illumination (Fig. 5a), whereas self-reduction barely occurred in dark. Surprisingly, the self-reduction process of Cu_2O was not continuously linear. It had an outbreak period from 2 h to 3 h, and stopped when the amount of self-reduced Cu accounted for 4.7 % of the total Cu content.

The simulated reaction solution sampled the suspension during the outbreak period of Cu_2O self-reduction (2 h light exposure). After $AgNO_3$ treatment, TEM observation was carried out on the treated sample. By tilting the sample 20° and -20°, three representative segments of the Cu_2O self-reduction were observed (Fig. 5b-d) and relative structure were identified (insert figure). At the early stage, Ag occupied 8 top corners of the Cu_2O cubes as shown in Fig. 5b. Subsequently, Ag not only occupied 8 top corners of the Cu_2O cubes, but also gradually stretched towards the edge (Fig. 5c). At the end, in Fig. 5d we can see that Ag particles were distributed on the top corner, edge and facet of the Cu_2O cubes. In order to further verify whether there was a temporal connection among these three segments, more TEM images and dark field images of Cu_2O samples at the beginning, middle and end of self-reduction were obtained. When Cu_2O self-reduction started (Figure S3), white spots represented Ag in dark field images mostly located at vertexes of Cu_2O cubes. When the self-reduction of Cu_2O entered the outbreak stage (Figure S4), the white bright spots in the dark field images gradually spread to the edges and facets Cu_2O cubes. When the self-reduction of Cu_2O reached saturated (Figure S5), Ag particles wrapped around Cu_2O cubes. Ag permutation could only occur in the position where Cu was, so the position of Ag could refer to the position where Cu was generated by the self-reduction of Cu_2O. Therefore, Cu_2O self-reduction occur at the vertexes of Cu_2O cubes first, then spreads to the edges, and finally occurs on the surfaces. According to the structure characterization of fresh Cu_2O samples, the vertexes, edges and surfaces of Cu_2O expose {111}, {110} and {100} crystal planes, respectively.

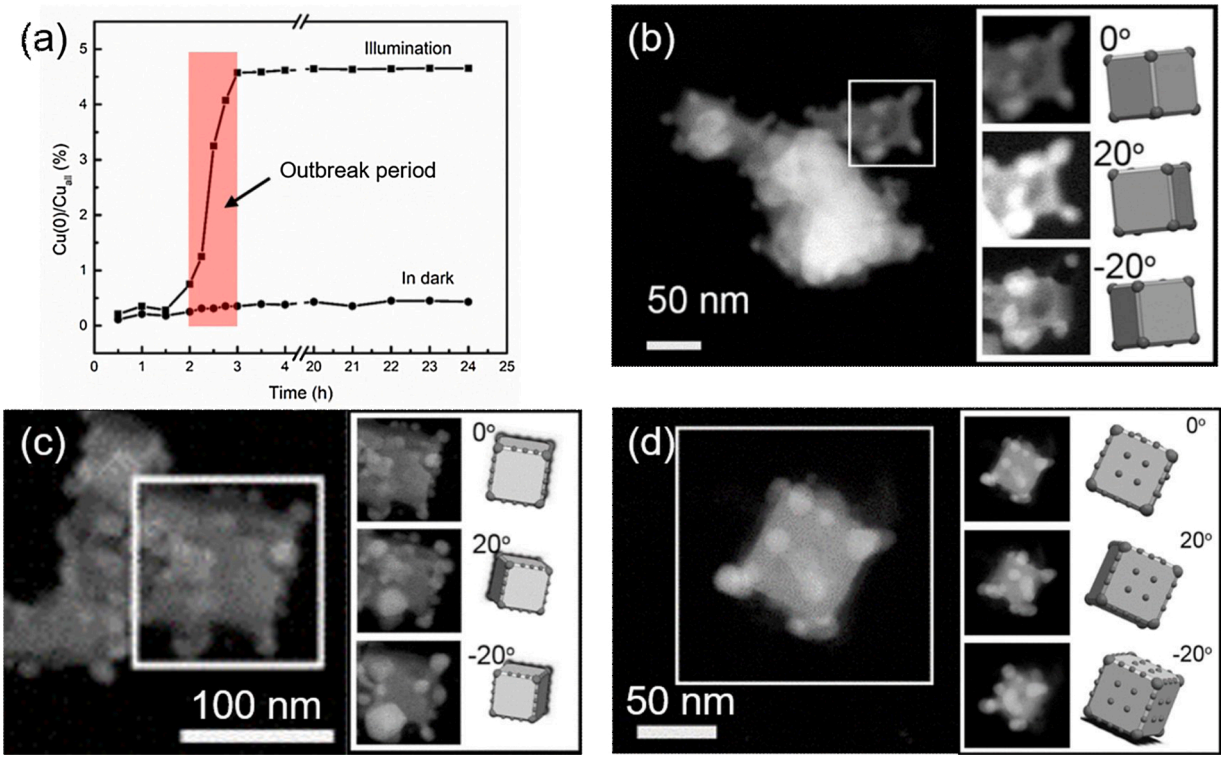

Fig. 5. (a) Quantitative results of Cu_2O self-reduction, scanning transmission electron microscope (STEM) images of reduced Cu_2O in outbreak period: (b) Ag located on 8 vertexes of Cu_2O cubes, (c) Ag located on both vertexes and edges of Cu_2O cubes, (d) Ag located on vertexes, edges and surfaces of Cu_2O cubes. All the STEM images were obtained after $AgNO_3$ treatment. Therefore, the positions of Ag were where Cu_2O self-reduced to Cu.

Therefore, the reasonable priority order of Cu_2O self-reduction is {111} > {110} > {100}.

Cu_2O self-reduction requires electrons. In order to explore the reasons of self-reduction priority on different exposed facets of Cu_2O, the lowest unoccupied molecular orbit (LUMO) energy of {111}, {110} and {100} facets were calculated. As showed in Fig. 6, the order of LUMO energy of different facets followed {111} < {110} < {100}. Photogenic electrons tend to deposit on the crystal surface with low LUMO energy. Hence, the priority order of photogenic electron deposition on facets of Cu_2O was {111} > {110} > {100}, which was consistent with the priority order of Cu_2O self-reduction. Considering a reduction reaction requires extra electrons, it was inferred that the accumulation of photogenic electrons on exposed facets of Cu_2O was the driving force of Cu_2O self-reduction.

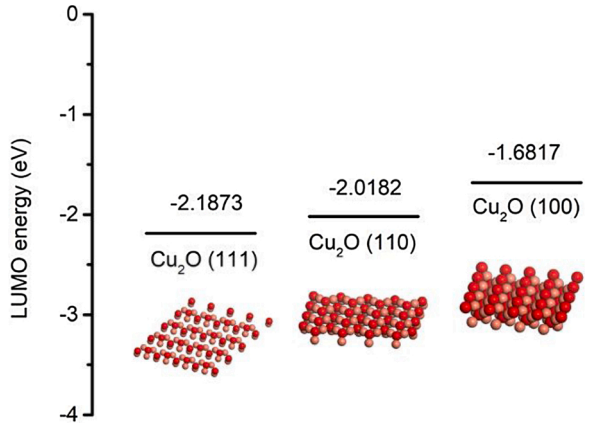

Fig. 6. LUMO energy of Cu_2O crystal planes.

3.4. Whether self-reduction is positive or negative

It was noted that the self-reduction process of Cu_2O was not continuously linear. When the amount of reduced Cu accounted for 4.7 % of the total Cu content, the self-reduction process stopped. If, as described in some literatures, [38,41] the formation of Cu would led to poisoning of Cu_2O catalyst, the photocatalytic activity of Cu_2O should remain constant when Cu_2O self-reduction stopped. However, the activity of Cu_2O in literatures [44,47,48] decreased gradually with the increase cycle runs of photocatalytic H_2 evolution, which contradicted the saturation value in the self-reduction process of Cu_2O. To explore the role of Cu_2O self-reduction, photocatalytic H_2 evolution performance on Cu_2O was investigated. As shown in Fig. 7, Cu_2O photocatalytic hydrogen production had an induction period of about 2 h. After 2 h, the hydrogen production rate raised quickly, and reached its maximum in 1 h, then within left 21 h of the test, the hydrogen production rate of Cu_2O almost kept constant. Surprisingly, the variation trend of hydrogen production rate with time was strikingly similar to the degree of Cu_2O self-reduction (Fig. 7b and c). The time when Cu_2O started to self-reduce coincided with the time when Cu_2O started to produce hydrogen. After the Cu_2O self-reduction stopped, the hydrogen production rate on the Cu_2O catalyst remained constant, and the total amount of hydrogen production increased linearly with time. Therefore, we speculate that nano-Cu generated on Cu_2O cubes are the active sites of photocatalytic hydrogen production.

Similar to Au and Ag, Cu has been reported to have a localized surface plasmon resonance effect. [44,49,50] Plasmonic nanostructures support the formation of resonant surface plasmons in response to a photon flux, localizing electromagnetic energy close to their surfaces. The interaction of localized electric fields with the neighboring semiconductor allows for the selective formation of electron/hole pairs in the near-surface region of the semiconductor [51–54]. Moreover, irradiating metal nanoparticles near their plasmon resonance frequency can generate intense local electric fields near the surface of the

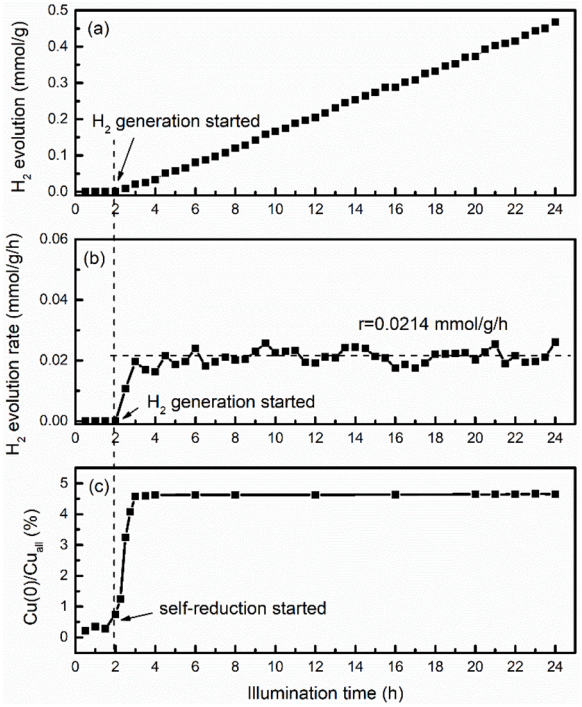

Fig. 7. (a) Cumulative H_2 evolution and (b) H_2 evolution rate on Cu_2O catalyst, and (c) quantitative results of Cu_2O self-reduction. (The photocatalytic hydrogen production rate on Cu_2O catalyst was estimated by the amount of hydrogen production per 30 min.).

nanoparticles. The electric field intensity of local plasmonic "hot spots" is much higher than the incident electric field, and thus, the electron-hole pair generation rate is accelerated [55–57]. Based on previous reports, a possible explanation for the role of Cu_2O self-reduction in photocatalytic hydrogen production was proposed. When Cu_2O is illuminated in an anaerobic environment, it was excited and generated photogenic electron-holes on its surface. The holes are consumed by the ethanol sacrifice agent in the reaction solution, whereas the photogenic electrons which cannot be consumed in the anaerobic environment were accumulated. Driven by the accumulation of photogenic electrons, Cu_2O was self-reduced to form nano-Cu. The newly generated nano-Cu further accelerates Cu_2O reduction due to its localized surface plasmon resonance effect, which is also the possible reason for the outbreak period of Cu_2O self-reduction. With the growth of Cu nano-particles, the tendency of photoelectron reducing Cu_2O decreased gradually. When Cu_2O self-reduction reaches saturation, photoelectron generation mainly participates in hydrogen generation reaction.

Considering that in the previous EPR experiment, it has been proved that Cu self-reduced by Cu_2O would be oxidized to CuO when it was exposed in air. If Cu could actually accelerate the generation of H_2, when oxygen was introduced, the activity of catalyst would be reduced. To verify the hypothesis mentioned above, we treated Cu_2O catalyst with different atmosphere in the photocatalytic hydrogen production cycle test. As shown in Fig. 8a, the activity of Ar protected Cu_2O catalyst remained consistent in the three H_2 evolution cycles. In the first cycle, there was a 2 h induction period of photocatalytic hydrogen production reaction, and the induction period was obviously shortened in the second and third cycles. It is speculated that Cu has been generated on the surface of Cu_2O in the first cycle, and the rate of H_2 production rate is accelerated throughout the second and third cycles. On the contrary, when the reaction solution containing Cu_2O was pretreated with air before the second and third cycles, the hydrogen production activity of the Cu_2O catalyst decreases, and induction period existed in each cycle test. In addition, EPR signal of Cu^{2+} ($g_{\perp} = 2.07$) [46] was detected in curve of the Cu_2O catalyst treated by air after 3 photocatalytic H_2 evolution cycles, whereas no EPR signal of Cu^{2+} was found in Ar protected Cu_2O catalyst (Fig. 8b). It is further verified that Cu self-reduced by Cu_2O is beneficial to photocatalytic hydrogen production. The catalyst exposure in air will lead to the oxidation of Cu, which was harmful to the photocatalytic hydrogen production on Cu_2O catalyst.

4. Conclusions

In this work, the in-situ formation of active site on Cu_2O catalyst under stimuli of light irradiation was observed through liquid cell TEM with light induced. Cu_2O cubes self-reduced to nano-Cu during photocatalytic H_2 evolution, and the sequence of self-reduction occurred on Cu_2O exposed facets followed {111} > {110} > {100}. The accumulation of photogenic electrons was supposed to be the driving force of Cu_2O self-reduction. The variation trend of hydrogen production rate with time was highly matched with the degree of nano-Cu formation, which indicated nano-Cu generated by self-reduction were the photocatalytic active sites. The localized surface plasmon resonance effect of Cu nanoparticles was considered to be the reason of excellent activity of Cu_2O catalysts. When exposed to air and the nano-copper oxidized, catalyst no longer have catalytic activity, which further confirmed the in-situ formed nano-Cu was the active site of reaction.

CRediT authorship contribution statement

Shuohan Yu: Conceptualization, Methodology, Validation,

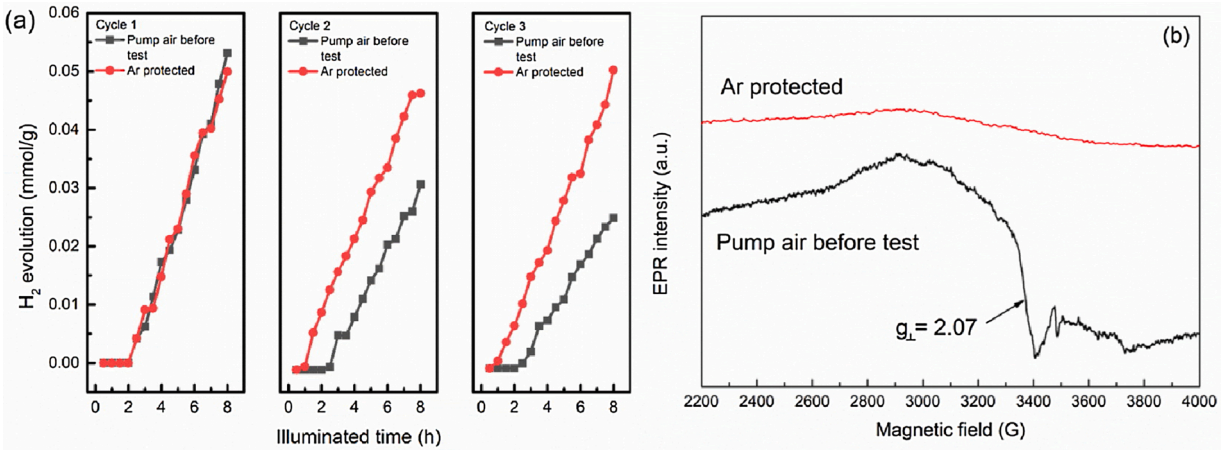

Fig. 8. (a) H_2 evolution on Cu_2O catalysts pretreated by different atmospheres, (b) EPR results of catalysts after photocatalytic test cycle 3.

Investigation, Writing - original draft, Funding acquisition. **Youhong Jiang:** Data curation, Validation, Investigation. **Yue Sun:** Investigation, Data curation. **Fei Gao:** Conceptualization, Methodology, Resources, Writing - review & editing, Supervision, Funding acquisition. **Weixin Zou:** Writing - review & editing, Data curation. **Honggang Liao:** Conceptualization, Methodology, Resources, Writing - review & editing, Supervision, Funding acquisition. **Lin Dong:** Conceptualization, Writing - review & editing, Funding acquisition, Project administration.

Declaration of Competing Interest

There are no conflicts of interest to declare.

Acknowledgements

This work was financially supported by Special Fund for Research on National Major Research Instruments of China (No. 21427803), National Key Research and Development Program of China (2017YFA0206500) and National Natural Science Foundation of China (Grant Nos. 21972063, 21673198, 91934303). Youth program of National Natural Science Foundation of China (No. 21902074) are gratefully acknowledged.

Appendix A. Supplementary data

Supplementary material related to this article can be found, in the online version, at doi:https://doi.org/10.1016/j.apcatb.2020.119743.

References

[1] X.-F. Yang, A. Wang, B. Qiao, J. Li, J. Liu, T. Zhang, Single-Atom Catalysts: A New Frontier in Heterogeneous Catalysis, Acc. Chem. Res. 46 (2013) 1740–1748.
[2] A. Haruta, When gold is not noble: catalysis by nanoparticles, Chem. Rec. 3 (2003) 75–87.
[3] J. Liu, L. Chen, H. Cui, J. Zhang, L. Zhang, C.-Y. Su, Applications of metal-organic frameworks in heterogeneous supramolecular catalysis, Chem. Soc. Rev. 43 (2014) 6011–6061.
[4] X. Zou, Y. Zhang, Noble metal-free hydrogen evolution catalysts for water splitting, Chem. Soc. Rev. 44 (2015) 5148–5180.
[5] M.S. Nasir, G. Yang, I. Ayub, S. Wang, L. Wang, X. Wang, W. Yan, S. Peng, S. Ramakarishna, Recent development in graphitic carbon nitride based photocatalysis for hydrogen generation, Appl. Catalysis B-Environ. 257 (2019).
[6] J. Xiong, P. Song, J. Di, H. Li, Ultrathin structured photocatalysts: a versatile platform for CO_2 reduction, Appl. Catalysis B-Environ. 256 (2019).
[7] C. Wen, A. Yin, W.-L. Dai, Recent advances in silver-based heterogeneous catalysts for green chemistry processes, Appl. Catalysis B-Environ. 160 (2014) 730–741.
[8] T. Ikeda, M. Boero, S.-F. Huang, K. Terakura, M. Oshima, J.-i. Ozaki, Carbon alloy catalysts: active sites for oxygen reduction reaction, J. Phys. Chem. C 112 (2008) 14706–14709.
[9] J. Kibsgaard, Z. Chen, B.N. Reinecke, T.F. Jaramillo, Engineering the surface structure of MoS_2 to preferentially expose active edge sites for electrocatalysis, Nat. Mater. 11 (2012) 963–969.
[10] M. Behrens, F. Studt, I. Kasatkin, S. Kuehl, M. Haevecker, F. Abild-Pedersen, S. Zander, F. Girgsdies, P. Kurr, B.-L. Kniep, M. Tovar, R.W. Fischer, J.K. Norskov, R. Schloegl, The active site of methanol synthesis over $Cu/ZnO/Al_2O_3$ industrial catalysts, Science 336 (2012) 893–897.
[11] T.F. Jaramillo, K.P. Jorgensen, J. Bonde, J.H. Nielsen, S. Horch, I. Chorkendorff, Identification of active edge sites for electrochemical H_2 evolution from MoS_2 nanocatalysts, Science 317 (2007) 100–102.
[12] J.H. Kwak, J. Hu, D. Mei, C.-W. Yi, D.H. Kim, C.H.F. Peden, L.F. Allard, J. Szanyi, Coordinatively unsaturated Al^{3+} centers as binding sites for active catalyst phases of platinum on gamma-Al_2O_3, Science 325 (2009) 1670–1673.
[13] M. Borasio, O.R. de la Fuente, G. Rupprechter, H.J. Freund, In situ studies of methanol decomposition and oxidation on Pd(111) by PM-IRAS and XPS spectroscopy, J. Phys. Chem. B 109 (2005) 17791–17794.
[14] S. Velu, K. Suzuki, C.S. Gopinath, Photoemission and in situ XRD investigations on CuCoZnAl-mixed metal oxide catalysts for the oxidative steam reforming of methanol, J. Phys. Chem. B 106 (2002) 12737–12746.
[15] M.J. Kale, P. Christopher, Utilizing quantitative in situ FTIR spectroscopy to identify well-coordinated Pt atoms as the active site for CO oxidation on Al_2O_3-Supported Pt catalysts, ACS Catal. 6 (2016) 5599–5609.
[16] S. Chenna, R. Banerjee, P.A. Crozier, Atomic-scale observation of the Ni activation process for partial oxidation of methane using in situ environmental TEM, Chemcatchem 3 (2011) 1051–1059.
[17] E.L. Lee, I.E. Wachs, In situ Raman spectroscopy of SiO_2-supported transition metal oxide catalysts: an isotopic O-18-O-16 exchange study, J. Phys. Chem. C 112 (2008) 6487–6498.
[18] H. Arakawa, M. Aresta, J.N. Armor, M.A. Barteau, E.J. Beckman, A.T. Bell, J. E. Bercaw, C. Creutz, E. Dinjus, D.A. Dixon, K. Domen, D.L. DuBois, J. Eckert, E. Fujita, D.H. Gibson, W.A. Goddard, D.W. Goodman, J. Keller, G.J. Kubas, H. H. Kung, J.E. Lyons, L.E. Manzer, T.J. Marks, K. Morokuma, K.M. Nicholas, R. Periana, L. Que, J. Rostrup-Nielson, W.M.H. Sachtler, L.D. Schmidt, A. Sen, G. A. Somorjai, P.C. Stair, B.R. Stults, W. Tumas, Catalysis research of relevance to carbon management: progress, challenges, and opportunities, Chem. Rev. 101 (2001) 953–996.
[19] S. Bordiga, E. Groppo, G. Agostini, J.A. van Bokhoven, C. Lamberti, Reactivity of surface species in heterogeneous catalysts probed by in situ X-ray absorption techniques, Chem. Rev. 113 (2013) 1736–1850.
[20] F. Besenbacher, I. Chorkendorff, B.S. Clausen, B. Hammer, A.M. Molenbroek, J. K. Norskov, I. Stensgaard, Design of a surface alloy catalyst for steam reforming, Science 279 (1998) 1913–1915.
[21] B. Roldan Cuenya, Synthesis and catalytic properties of metal nanoparticles: size, shape, support, composition, and oxidation state effects, Thin Solid Films 518 (2010) 3127–3150.
[22] P.J. Ferreira, G.J. la O, Y. Shao-Horn, D. Morgan, R. Makharia, S. Kocha, H. A. Gasteiger, Instability of Pt/C electrocatalysts in proton exchange membrane fuel cells - A mechanistic investigation, J. Electrochem. Soc. 152 (2005) A2256–A2271.
[23] A. Liu, L. Liu, Y. Cao, J. Wang, R. Si, F. Gao, L. Dong, Controlling dynamic structural transformation of atomically dispersed CuOx species and influence on their catalytic performances, ACS Catal. 9 (2019) 9840–9851.
[24] F.M. Toma, J.K. Cooper, V. Kunzelmann, M.T. McDowell, J. Yu, D.M. Larson, N. J. Borys, C. Abelyan, J.W. Beeman, K.M. Yu, J. Yang, L. Chen, M.R. Shaner, J. Spurgeon, F.A. Houle, K.A. Persson, I.D. Sharp, Mechanistic insights into chemical and photochemical transformations of bismuth vanadate photoanodes, Nat. Commun. 7 (2016).
[25] B. Weng, M.-Y. Qi, C. Han, Z.-R. Tang, Y.-J. Xu, Photocorrosion inhibition of semiconductor-based photocatalysts: basic principle, current development, and future perspective, ACS Catal. 9 (2019) 4642–4687.
[26] W. Zhen, X. Ning, B. Yang, Y. Wu, Z. Li, G. Lu, The enhancement of CdS photocatalytic activity for water splitting via anti-photocorrosion by coating Ni_2P shell and removing nascent formed oxygen with artificial gill, Appl. Catalysis B-Environ. 221 (2018) 243–257.
[27] M.-Q. Yang, C. Han, Y.-J. Xu, Insight into the effect of highly dispersed MoS_2 versus layer-structured MoS_2 on the photocorrosion and photoactivity of CdS in Graphene-CdS-MoS_2 composites, J. Phys. Chem. C 119 (2015) 27234–27246.
[28] H.-G. Liao, H. Zheng, Liquid cell transmission Electron microscopy study of platinum Iron nanocrystal growth and shape evolution, J. Am. Chem. Soc. 135 (2013) 5038–5043.
[29] J. Yang, Z. Zeng, J. Kang, S. Betzler, C. Czarnik, X. Zhang, C. Ophuss, C. Yu, K. Bustillo, M. Pan, J. Qiu, L.-W. Wang, H. Zheng, Formation of two-dimensional transition metal oxide nanosheets with nanoparticles as intermediates, Nat. Mater. 18 (2019), 970-+.
[30] Z.-W. Yin, S.B. Betzler, T. Sheng, Q. Zhang, X. Peng, J. Shangguan, K.C. Bustillo, J.-T. Li, S.-G. Sun, H. Zheng, Visualization of facet-dependent pseudo-photocatalytic behavior of TiO_2 nanorods for water splitting using in situ liquid cell TEM, Nano Energy 62 (2019) 507–512.
[31] Y. Lu, W.-J. Yin, K.-L. Peng, K. Wang, Q. Hu, A. Selloni, F.-R. Chen, L.-M. Liu, M.-L. Sui, Self-hydrogenated shell promoting photocatalytic H_2 evolution on anatase TiO_2, Nat. Commun. 9 (2018).
[32] C.-H. Kuo, C.-H. Chen, M.H. Huang, Seed-mediated synthesis of monodispersed Cu_2O nanocubes with five different size ranges from 40 to 420 nm, Adv. Funct. Mater. 17 (2007) 3773–3780.
[33] G. Kresse, J. Furthmüller, Efficient iterative schemes for ab initio total-energy calculations using a plane-wave basis set, Phys. Rev. B 54 (1996) 11169–11186.
[34] G. Kresse, J. Hafner, Ab initio, Phys. Rev. B 49 (1994) 14251–14269.
[35] P.E. Blöchl, Projector augmented-wave method, Phys. Rev. B 50 (1994) 17953–17979.
[36] J.P. Perdew, K. Burke, M. Ernzerhof, Generalized gradient approximation made simple, Phys. Rev. Lett. 77 (1996) 3865–3868.
[37] H.J. Monkhorst, J.D. Pack, Special points for Brillouin-zone integrations, Phys. Rev. B 13 (1976) 5188.
[38] C.Y. Toe, J. Scott, R. Amal, Y.H. Ng, Recent advances in suppressing the photocorrosion of cuprous oxide for photocatalytic and photoelectrochemical energy conversion, J. Photochem. Photobiol. C-Photochem. Rev. 40 (2019) 191–211.
[39] S. Kakuta, T. Abe, Structural characterization of Cu_2O after the evolution of H_2 under visible light irradiation, Electrochem. Solid State Lett. 12 (2009) P1–P3.
[40] C.Y. Toe, Z. Zheng, H. Wu, J. Scott, R. Amal, Y.H. Ng, Photocorrosion of cuprous oxide in hydrogen production: rationalising self-oxidation or self-reduction, Angewandte Chemie Int. Ed. 57 (2018) 13613–13617.
[41] C.-M. Wang, C.-Y. Wang, Photocorrosion of plasmonic enhanced Cu_xO photocatalyst, J. Nanophotonics 8 (2014).
[42] P.D. Tran, S.K. Batabyal, S.S. Pramana, J. Barber, L.H. Wong, S.C.J. Loo, A cuprous oxide-reduced graphene oxide (Cu_2O-rGO) composite photocatalyst for hydrogen generation: employing rGO as an electron acceptor to enhance the photocatalytic activity and stability of Cu_2O, Nanoscale 4 (2012) 3875–3878.
[43] W. Zhen, W. Jiao, Y. Wu, H. Jing, G. Lu, The role of a metallic copper interlayer during visible photocatalytic hydrogen generation over a $Cu/Cu_2O/Cu/TiO_2$ catalyst, Catal. Sci. Technol. 7 (2017) 5028–5037.
[44] Y. Lou, Y. Zhang, L. Cheng, J. Chen, Y. Zhao, A stable plasmonic $Cu@Cu_2O/ZnO$ heterojunction for enhanced photocatalytic hydrogen generation, Chemsuschem 11 (2018) 1505–1511.

[45] R. Li, X. Tao, R. Chen, F. Fan, C. Li, Synergetic effect of dual Co-catalysts on the activity of p-Type Cu2O crystals with anisotropic facets, Chem. Eur. J. 21 (2015) 14337–14341.
[46] G. Pourroy, S. Angelov, ESR study of CuO-Doped cordierite, J. Mater. Sci. 27 (1992) 6730–6734.
[47] Z. Li, J. Liu, D. Wang, Y. Gao, J. Shen, $Cu_2O/Cu/TiO_2$ nanotube Ohmic heterojunction arrays with enhanced photocatalytic hydrogen production activity, Int. J. Hydrogen Energy 37 (2012) 6431–6437.
[48] Q.M. Wang, Y.M. Lin, K.G. Liu, Role of anions associated with the formation and properties of silver clusters, Acc. Chem. Res. 48 (2015) 1570.
[49] E. Liu, L. Qi, J. Bian, Y. Chen, X. Hu, J. Fan, H. Liu, C. Zhu, Q. Wang, A facile strategy to fabricate plasmonic Cu modified TiO_2 nano-flower films for photocatalytic reduction of CO_2 to methanol, Mater. Res. Bull. 68 (2015) 203–209.
[50] J.S. Sekhon, S.S. Verma, Refractive index sensitivity analysis of Ag, Au, and Cu nanoparticles, Plasmonics 6 (2011) 311–317.
[51] S.K. Cushing, J. Li, F. Meng, T.R. Senty, S. Suri, M. Zhi, M. Li, A.D. Bristow, N. Wu, Photocatalytic activity enhanced by plasmonic resonant energy transfer from metal to semiconductor, J. Am. Chem. Soc. 134 (2012) 15033–15041.
[52] R. Jiang, B. Li, C. Fang, J. Wang, Metal/Semiconductor hybrid nanostructures for plasmon-enhanced applications, Adv. Mater. 26 (2014) 5274–5309.
[53] M. Liu, Nd.L. Snapp, H. Park, Water photolysis with a cross-linked titanium dioxide nanowire anode, Chem. Sci. 2 (2011) 80–87.
[54] T. Tatsuma, H. Nishi, T. Ishida, Plasmon-induced charge separation: chemistry and wide applications, Chem. Sci. 8 (2017) 3325–3337.
[55] C. Tira, D. Tira, T. Simon, S. Astilean, Finite-Difference Time-Domain (FDTD) design of gold nanoparticle chains with specific surface plasmon resonance, J. Mol. Struct. 1072 (2014) 137–143.
[56] M. Bernardi, J. Mustafa, J.B. Neaton, S.G. Louie, Theory and computation of hot carriers generated by surface plasmon polaritons in noble metals, Nat. Commun. 6 (2015).
[57] W. Hou, S.B. Cronin, A review of surface plasmon resonance-enhanced photocatalysis, Adv. Funct. Mater. 23 (2013) 1612–1619.